Process Safety and Environmental Protection 194 (2025) 1421–1433

Contents lists available at ScienceDirect

Process Safety and Environmental Protection

journal homepage: www.journals.elsevier.com/process-safety-and-environmental-protection

Process Optimization And Life Cycle Assessment In a 10MWth food waste chemical looping gasification system for hydrogen production

Mingyang Dai [b], Qiuyan Xue [c], Tuo Guo [a,d,*], Qingjie Guo [a,b,*]

[a] Laboratory of Green & Smart Chemical Engineering in Universities of Shandong, College of Chemical Engineering, Qingdao University of Science & Technology, Qingdao, Shandong 266042, China
[b] Center of carbon capture and industrial utilization, Jiangmen Laboratory of Carbon Science and Technology, Jiangmen 529020, China
[c] State Key Laboratory of Coal Efficient Utilization and Green Chemical Engineering, College of Chemistry and Chemical Engineering, National Experimental Teaching Demonstration Center of Chemistry, Ningxia University, Yinchuan, Ningxia 750021, China
[d] Xinyuan Green Carbon Technology (Jiangmen) Co., Ltd, Jiangmen 529199, China

ARTICLE INFO

Keywords:
Food waste
Chemical looping gasification
Aspen plus
Economic analysis
Life cycle assessment

ABSTRACT

The present study involved an in-depth simulation and evaluation of a 10 MW_{th} food waste chemical looping gasification to hydrogen system, conducted using Aspen Plus process simulation software. The study extensively investigated process optimization, economic evaluation, and the environmental impacts associated with the application of this technology. The simulation results showed that maintaining a fuel reactor temperature at 850°C, an H_2O/C ratio of 0.6, and an O/C of 0.45 yielded an H_2/CO of 1.718, Y of 1.209 m^3/kg, and CEG of 51.78 %. Life cycle assessment indicated favorable outcomes concerning environmental impacts. Particularly, the system operational in the Qingdao region showed a global warming potential of 1763.5 $kgCO_{2\text{-eq}}$ and an acidification potential of 16.77 $kgSO_{2\text{-eq}}$. Economic analysis revealed that the system offers substantial economic benefits with a return on investment of 11.23 %, a payback period of 6.283 years, and a net present value of 1.201×10^6 $. The cost of this process significantly undercuts that of renewable hydrogen production, providing considerable environmental advantages by effectively utilizing waste resources and reducing waste disposal issues. Given its cost-effectiveness and environmental benefits, chemical looping gasification technology for hydrogen production from food waste holds wide-ranging future application potential.

1. Introduction

As global population growth continues and urbanization accelerates, the production of food waste (FW) has increased dramatically, emerging as a significant environmental challenge worldwide (Dhiman and Mukherjee, 2021). It is estimated that over 1.3 billion t of FW are generated globally each year. This not only leads to a substantial waste of resources but also creates significant environmental issues during disposal, such as greenhouse gas emissions, water pollution, and soil degradation (Saqib et al., 2019). According to relevant statistics, China generates approximately 80 million t of FW annually, with an annual growth rate of 10 %. Food waste decomposes easily, producing foul odors and significantly impacting human health and the environment. Due to its high organic content, which accounts for over 90 % of the dry matter, and its high moisture content and rich organic composition, the treatment and efficient utilization of FW present increasing challenges (Havukainen et al., 2017; Tang et al., 2012; Zhou et al., 2014). Currently, FW is often managed through techniques such as composting, anaerobic digestion, incineration, or landfilling (Jin et al., 2021). However, traditional methods such as landfilling, incineration, and anaerobic digestion have limitations in effectively treating FW. The options for disposing of waste in landfills are limited due to the scarcity of land resources. Incineration requires a considerable amount of additional fuel and significant financial investment. Anaerobic digestion, on the other hand, is characterized by low efficiency, long operational periods, and the potential to cause environmental damage (Caton et al., 2010; Chen et al., 2019). Therefore, identifying effective techniques for the treatment and resource recovery of food waste has become a crucial research direction in the fields of environmental protection and sustainable development.

* Corresponding authors at: Laboratory of Green & Smart Chemical Engineering in Universities of Shandong, College of Chemical Engineering, Qingdao University of Science & Technology, Qingdao, Shandong 266042, China.
E-mail addresses: tuo.guo.20@alumni.ucl.ac.uk (T. Guo), qingjie_guo@vip.sina.com (Q. Guo).

https://doi.org/10.1016/j.psep.2024.12.103
Received 11 August 2024; Received in revised form 6 December 2024; Accepted 26 December 2024
Available online 27 December 2024

FW gasification is a thermal process that transforms organic waste into syngas by exposing it to high temperatures. By using dry FW as a fuel source in the gasification process, the organic elements of FW are converted into reusable solid byproducts and syngas, primarily composed of CO, H_2, and CH_4. This syngas can be utilized for electricity generation, heating, or as a raw material for chemical production (Matsakas et al., 2017). However, gasification technology presents certain drawbacks, including high costs, technical complexity, potential environmental pollution (for example, emissions of HCl and H_2S), stringent pre-treatment requirements for feedstock, and the risk of secondary pollution from the handling of residuals (Shahabuddin et al., 2020). Compared to traditional FW gasification, Chemical Looping Gasification (CLG) offers significant advantages in FW treatment. Firstly, CLG employs oxygen carriers (OC) instead of air to supply oxygen, which prevents nitrogen from entering the system, thereby significantly enhancing the purity and calorific value of the syngas (Yu et al., 2019). Moreover, in the CLG process, OC can be recycled, significantly reducing the consumption of auxiliary fuel and operating costs (Dieringer et al., 2020). Additionally, CLG effectively minimizes the production of harmful gases such as HCl and H_2S, thereby reducing the risk of environmental pollution (Jiang et al., 2022). Due to the relatively low requirements of CLG for the moisture content and particle size of FW, the pre-treatment process is simpler, thereby reducing operational complexity and cost (Molino et al., 2016) Additionally, the residue produced by CLG primarily consists of OC and a small amount of non-combustible material. This residue is less toxic and easier to handle, further reducing the risk of secondary pollution (Tahir et al., 2023). Therefore, CLG demonstrates significant advantages in enhancing gasification efficiency, reducing environmental pollution, and simplifying operations.

Many researchers have conducted in-depth studies on the resourceful treatment of FW. Tanaka et al. (Tanaka et al., 2008) were the first to explore FW gasification technology using steam as a gasifying agent for hydrogen production. The findings indicate that FW gasification is highly effective in minimizing the production of residual waste. Ahmed et al. (Ahmed and Gupta, 2010) conducted a study demonstrating that steam gasification of FW is more efficient than the pyrolysis method. This technique significantly enhances the production of syngas and hydrogen. Although these tests highlight the potential of gasification technology in FW treatment, they also reveal limitations. For example, these studies did not thoroughly examine the impact of key process parameters on gasification technology, leading to relatively idealized conclusions.

Xu et al. (Xu et al., 2023) conducted an analysis of energy efficiency, techno-economics, and environmental impact by integrating plasma gasification with chemical looping technology using FW as feedstock. The study found that plasma gasification exhibits high energy efficiency and low environmental impact, but its substantial cost necessitates a careful balance in practical applications. Menacho et al. (Menacho et al., 2022) engaged in simulation modeling and analysis to explore the process of biogas production from food waste. They investigated the influence of various operational parameters on biogas yield. The results indicated that optimizing temperature and pressure significantly affects the quantity and quality of biogas produced, providing valuable theoretical support for future large-scale implementation. Sun et al. (Sun et al., 2024) performed a comprehensive performance analysis comparing the co-gasification of food waste and municipal solid waste. Their research showed that co-gasifying various types of biomass could enhance syngas production and improve the stability and efficiency of the gasification process. Ramzan et al. (Ramzan et al., 2011) developed a steady-state simulation model to accurately simulate the co-gasification of multiple biomass sources, including food waste, municipal solid waste, and chicken manure. This study used the Gibbs free energy minimization technique to assess the impact of various parameters, such as temperature, equivalence ratio, biomass moisture content, and steam injection, on the composition of syngas, its calorific value, and the efficiency of cold gas production. The findings revealed that higher temperatures promote the formation of CO and H_2, while higher equivalence ratios reduce the synthesis of these gases, leading to decreased cold gas efficiency. Currently, the primary focus of resource utilization for FW is on the gasification step, yet comprehensive assessments of the CLG process for FW are scarce. This gap complicates the quantitative analysis of the environmental and economic impacts of the FWCLG process.

The effective transformation of FW into high-quality energy remains a crucial field of study. However, most research is still in the experimental phase, and there is a notable lack of publications on process modeling, lifecycle assessment, and economic evaluation of FWCLG for hydrogen generation. This study uses Aspen Plus software to analyze the 10 MW_{th} FWCLG process. The goal is to effectively convert food waste into hydrogen-rich syngas using chemical looping gasification technology. Through sensitivity analysis, the optimal operating parameters of the system can be identified. The application of lifecycle assessment and economic analysis methods aims to minimize the production of harmful substances and maximize the environmental and economic benefits of the process. This study provides theoretical validation for the effective utilization and environmentally responsible management of freshwater resources, offering guidance for future technical advancements and industrial implementation.

2. Process description and gasification evaluation indicators

In this study, the FWCLC process was simulated using Aspen Plus V12. The complete procedure comprises four primary stages: drying, pyrolysis, CLG, and separation. The critical phase, CLG, involves extracting energy from food waste and converting it into gaseous molecules. Aspen Plus utilizes various thermodynamic property methods to evaluate parameters such as K-values, enthalpy, and density. (Al-Malah, 2022). The simulation adopted a property approach based on conventional components due to the consistency of physical property methods for solid components. Given the presence of traditional components operating at low pressure, the PENG-ROB property method was selected, as it is well-suited for applications in gas processing, refining, and petrochemicals. During the simulation, FW and ash were identified as non-traditional constituents. Since they cannot be represented with molecular formulae, the HCOALGEN and DCOALIGT models were employed to calculate the enthalpy and density of FW and ash. The stream type selected was MIXCINC.

To ensure the accuracy of the model, the following assumptions were primarily considered:

1. The FWCLG system operates under absolute pressure and is in a steady state.
2. Heat loss within the reactor is neglected.
3. Char is primarily composed of carbon and ash.
4. The impact of tar in high-temperature circumstances is disregarded.
5. The ash from FW is considered inert and does not participate in the gasification reactions.

In the CLG process, the system primarily consists of the Fuel Reactor (FR) and the Air Reactor (AR). In the FR, FW undergoes gasification with the release of lattice oxygen from the OC aided by steam, while the OC is reduced. Within the AR, the reduced OC reacts with the surrounding air and is rapidly regenerated to its original state. Compared to these reactions, the gasification of char and the reduction rate of OC are relatively low. Hence, it can be deduced that the rate-determining stages of the reaction in chemical looping technology predominantly occur in the FR. Furthermore, the reactions in the FR are highly complex. To accurately replicate this intricate procedure, a process model was developed using Aspen Plus, as illustrated in Fig. 1. The descriptions of each module in the simulation process are detailed in Table 1.

Due to the high C_p of water, excessive moisture content increases the

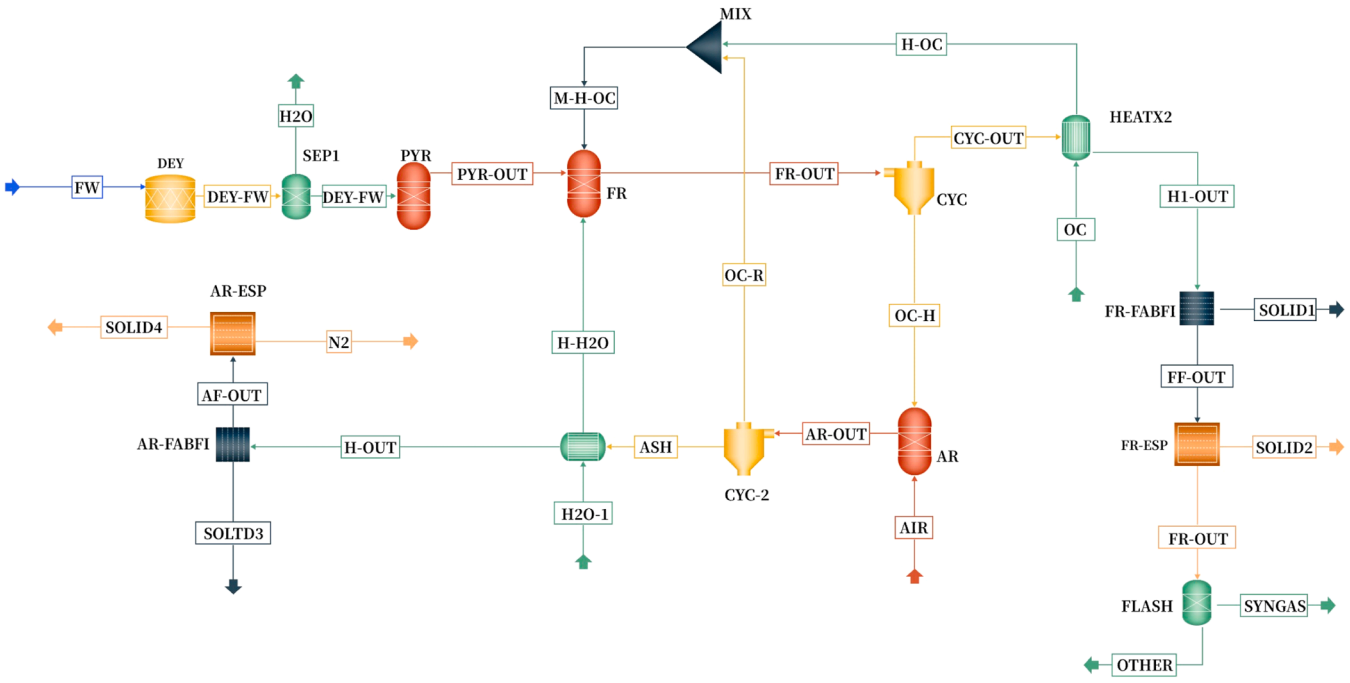

Fig. 1. Process Flow Diagram of the FWCLG System.

Table 1
Description of Process Modules in the FWCLG System.

nicknames	Module name	Descriptions
DEY	RStoic	A reactor model is used to decrease the water content of a sample by specifying its stoichiometric reaction, even while the reaction kinetics are unknown.
PYR	RYield	The stoichiometry and kinetics of the reactor model remain unknown, while the yield distribution data are known. The pyrolysis stage is employed to convert unconventional samples to their conventional elements.
FR、AR	RGibbs	The reactor lacks knowledge of the stoichiometry of the reaction, thus the equilibrium of the phases can be determined based on the minimization of the Gibbs free energy. This can be employed to simulate combustion or oxidation phases.
MIX	Mixer	It is necessary to combine the fluids that originate from each reactor module and proceed to the subsequent reactor.
CYC	Cyclone	The initial separation of OC is achieved through the use of a cyclone separator.
HEATX	HeatX	The objective is to achieve the greatest possible energy efficiency through the transfer of heat between flow strands.
FABFI	FabFl	The baghouse module is simulated as a gas-solid separator, with the objective of removing ash and small particles of OC from the syngas.
ESP	ESP	The module simulates a dry electrostatic precipitator, which is used to remove ash and small particles of OC and small particles of OC from the syngas.

energy consumption of the equipment. Therefore, FW is introduced into the drying reactor (DEY) at ambient temperature (25°C, 1 bar) to reduce its moisture content. The dried product then enters a flash separator (SEP-1) to yield streams of dry FW and water vapor. This separator operates under standard atmospheric pressure and feed temperature, using the thermodynamic principle of flash separation to effectively isolate the moisture. Due to the challenges in quantifying the Gibbs free energy of FW, it initially undergoes pyrolysis, leading to the separation of its elemental components: C, H_2, O_2, S, N_2, and ash. The pyrolysis process is simulated using a RYIELD reactor, which transforms uncommon components into conventional ones by determining the component product distribution. This reactor operates at a temperature of 600°C and a pressure of 1 bar. Subsequently, the degraded substances combine with OC and steam in the FR. The reaction occurs at a temperature of 850°C and a pressure of 1 bar. The reactions involving OC in the FR can be represented as follows: Fe_2TiO_5 ($Fe_2O_3 + TiO_2$) → $FeTiO_3$, and Fe_2O_3 → Fe_3O_4. However, given the imprecise description of ilmenite in Aspen Plus, the reaction involving ilmenite can be approximated to that of Fe_2O_3. The relevant reactions are listed below:

$$CO + 3Fe_2O_3 \rightarrow CO_2 + 2Fe_3O_4\# \quad (1)$$

$$H_2 + 3Fe_2O_3 \rightarrow H_2O + 2Fe_3O_4\# \quad (2)$$

$$CH_4 + 12Fe_2O_3 \rightarrow CO_2 + 2H_2O + 8Fe_3O_4\# \quad (3)$$

$$2C + 2CO_2 \Leftrightarrow 4CO\# \quad (4)$$

$$2C + 2H_2O \Leftrightarrow 2CO + 2H_2\# \quad (5)$$

$$CH_4 + H_2O \Leftrightarrow CO + 3H_2\# \quad (6)$$

$$2CH_4 + 2CO_2 \Leftrightarrow 4CO + 4H_2\# \quad (7)$$

$$CO + H_2O \Leftrightarrow H_2 + CO_2\# \quad (8)$$

$$CO + 3H_2 \Leftrightarrow CH_4 + H_2O\# \quad (9)$$

$$CO_2 + 4H_2 \Leftrightarrow CH_4 + 2H_2O\# \quad (10)$$

The model includes two cyclone separators (CYC), two baghouse filters (FABFI), a flash tank (FLASH), and two sets of heat exchangers. These components are utilized for gas-solid separation, pollutant absorption, steam condensation, and heat exchange between hot and cold streams. For the simulation, FW from the Qingdao area was selected as the fuel, and FW from various regions was also chosen as feedstock to enable comparisons of hydrogen production efficiency across different areas. The elemental and industrial analysis results are presented in Table 2. Natural ilmenite from Jiangsu, China, served as the OC. This material is cost-effective, readily available, and possesses a strong oxygen-carrying capacity, making it ideal for industrial use as an OC.

Table 2
Proximate and Ultimate Analysis of FW from Different Regions (Xu et al., 2022).

Sample	Proximate analysis (ad , ω/%)				ultimate analysis (ad , ω/%)					LHV/(MJ·kg^{-1})
	A	M	V	FC	C	H	O	N	S	
Qingdao	3.23	10.37	72.02	14.36	40.98	7.89	44.71	2.49	0.68	15.34
Beijing	11.3	8.2	66.7	13.8	42.34	4.8	34.36	6.7	0.5	14.53

The composition analysis of ilmenite is detailed in Table 3. When the total thermal input power of the system is 10 MW, the feed rate of FW is 782.08 kg/h. All stream inlet temperatures are set at 25°C, and the pressure is maintained at 1 bar. Under these conditions, the evaluation metrics for the system are established as follows:

The syngas yield Y (m^3/kg) refers to the volume of syngas produced per unit mass of biomass feedstock gasified at 25°C and 1 standard atmosphere. The calculation method is shown in Eq. (11):

$$Y = \frac{q_{syngas} \times V_l}{m_{biomass}} \# \tag{11}$$

Where q_{syngas} represents the molar flow rate of the total gas, in kmol/h; $m_{biomass}$ represents the mass flow rate of the biomass, in kg/h; and V_l is the molar volume of gas at standard conditions, which is 2.24×10^{-2}/(m^3/mol).

The hydrogen to carbon monoxide ratio (H_2/CO) of syngas is defined as the molar flow ratio of H_2 to CO. The calculation formula is shown in Eq. (12):

$$\frac{H_2}{CO} = \frac{q_{H2}}{q_{co}} \# \tag{12}$$

Where q_i represents the molar flow rate of the syngas component (kmol/h); represents H_2 and CO.

The lower heating value (LHV) of syngas (LHV_{syngas}, MJ/m^3) is defined as the chemical energy per cubic meter of syngas. The calculation method is shown in Eq. (13):

$$LHV_{syngas} = 12.64w_{CO} + 10.8w_{H_2} + 35.8w_{CH_4} \# \tag{13}$$

where w_i represents the mass fraction of each syngas component.

The cold gas efficiency (CGE, %) is defined as the ratio of the chemical energy contained in the syngas to the total energy of the biomass. The calculation formula is shown in Eq. (14):

$$CGE(\%) = \frac{m_{i,syngas} \times LHV_{i,syngas}}{m_{biomass} \times LHV_{biomass}} \times 100\% \# \tag{14}$$

where $LHV_{i,\ syngas}$ and $m_{i,\ syngas}$ represent the low level calorific value (MJ/kg) and mass flow rate (kg/h) of component i of the synthesis, respectively, and $LHV_{i,\ syngas}$ and $m_{i,\ syngas}$ represent the low level calorific value (MJ/kg) and mass flow rate (kg/h) of the biomass, respectively.

3. Results and discussions

3.1. Model validation

Currently, there are no reported experimental data for MW_{th}-scale FWCLG systems, making it difficult to directly verify the reliability of the FWCLG process model. Therefore, data and simulation results from previous experiments with a laboratory-scale fluidized bed reactor conducted by our team were selected for validation. Guo et al. (Wang et al., 2018). conducted FWCLG studies in a laboratory fluidized bed using Fe-based OC. In this study, the process model was validated under identical operating conditions: an O/C of 0.5, a steam flow rate of 1.0 g/min, a gasification temperature of 900°C, and gas concentrations expressed in molar percentages. As shown in Fig. 2, the deviations in H_2 selectivity, CO selectivity, CH_4 selectivity, and CO_2 selectivity from the experimental data were 3.93 %, 3.36 %, 2.91 %, and 4.38 %, respectively. The experimental data closely matched the simulation results, confirming the effectiveness of the constructed Aspen Plus model in replicating the FWCLG process. Therefore, this model is suitable for conducting further simulations under various conditions.

3.2. Sensitivity analysis

3.2.1. Effect of gasification temperature

Fig. 3 illustrates the trends in the molar fractions of syngas components, CGE, and H_2/CO during the hydrogen production process from FW in Qingdao as the fuel reactor temperature increases from 750°C to 950°C. Fig. 3**(a)** shows that the molar fractions of H_2 and CO gradually increase with rising temperature, while those of CO_2 and CH_4 decrease. This is because higher temperatures enhance reactions (4) and (5), leading to more H_2 and CO production. Additionally, at elevated temperatures, CH4 more readily decomposes into H_2 and CO ($CH_4 + H_2O \rightarrow CO + 3\ H_2$), resulting in a reduced molar fraction of CH_4. Furthermore, the high moisture and protein content of FW in Qingdao, due to the abundance of seafood and agricultural products, also supports the generation of H_2 and CO at higher temperatures (Xu et al., 2022).

Additionally, Fig. 3**(b)** illustrates that CGE increases with rising temperature, peaking at 950°C. This increase is attributed to higher

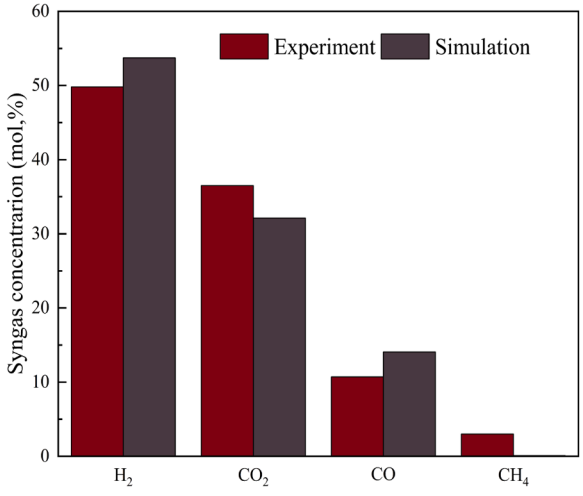

Fig. 2. Comparison of Experimental Data Reported by Guo et al. (Wang et al., 2018) and Simulation Data.

Table 3
Chemical composition of OC in natural ilmenite(Yuan et al., 2023).

Sample/ω%	Fe_2O_3	TiO_2	SiO_2	Al_2O_3	CaO	MgO	Na_2O	other
Ilmenite	46.76	25.22	13.49	5.6	4.73	1.95	0.85	1.4

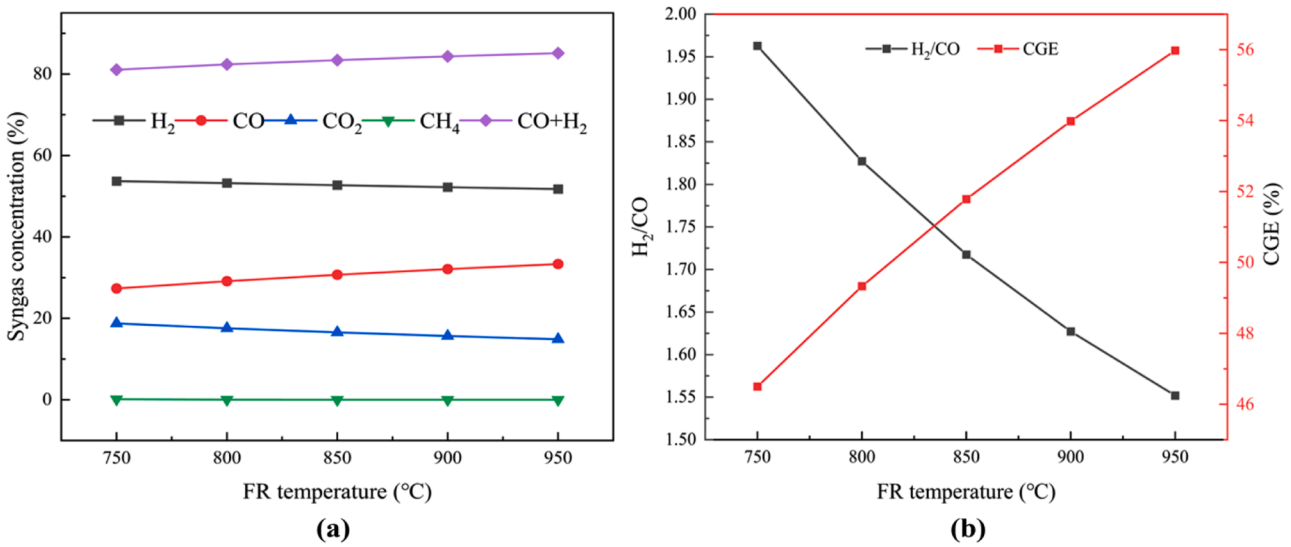

Fig. 3. Effect of FR Temperature on (a) Syngas Concentration, (b) H_2/CO, and CGE.

temperatures facilitating a more efficient conversion of feedstock into combustible gases, thereby enhancing CGE (Li et al., 2019). However, the H_2/CO decreases with increasing temperature due to the equilibrium shifts of the water-gas shift reaction and the reverse water-gas shift reaction at high temperatures (Desgagnés et al., 2024). The kinetics and thermodynamic properties of these reactions favor the production of more CO over H_2 under high-temperature conditions, leading to a decrease in the H_2/CO. This accounts for the reduction in the H_2/CO in syngas as the fuel reactor temperature increases from 750°C to 950°C.

Overall, the rise in temperature significantly promotes the generation of valuable gases and improves energy efficiency in the FWCLG process in the Qingdao region. Higher temperatures not only accelerate the decomposition and reactions of organic matter but also enhance CGE and hydrogen production, optimizing the economic viability and feasibility of the hydrogen production process. However, higher temperatures also entail greater energy consumption and more stringent equipment requirements. A temperature of 850°C provides a balance, maintaining high efficiency while minimizing energy consumption and operational costs, thereby maximizing economic benefits.

3.2.2. *Effect of H_2O/C*

Fig. 4 demonstrates the trends in the molar fractions of syngas components, CGE, and the H_2/CO during the CLG process of FW as the H_2O/C increases from 0.3 to 1.0. In Fig. 4**(a)**, it is observed that as the H_2O/C increases, the molar fraction of H_2 gradually rises, attributed to the enhancement of both the water-gas reaction and the water-gas shift reaction, which generate more H_2. Conversely, the molar fraction of CO gradually decreases because the elevated H_2O/C promotes the water-gas shift reaction, converting CO into CO_2 and H_2. As the molar fraction of CO decreases, that of CO_2 increases due to the enhanced conversion of CO to CO_2. The molar fraction of CH_4 shows little change, and may slightly decrease, as higher H_2O/C may inhibit CH_4 formation (Zhang et al., 2024). Additionally, the combined molar fraction of CO and H_2 shows a decreasing trend with increasing H_2O/C, primarily because the increase in H_2 does not fully compensate for the significant decrease in CO, resulting in an overall decrease.

Fig. 4**(b)** illustrates that CGE gradually decreases with an increasing H_2O/C. This decrease occurs because the introduction of more steam into the system absorbs substantial reaction heat, thus reducing the efficiency of the gasification reaction. This reduced gasification efficiency

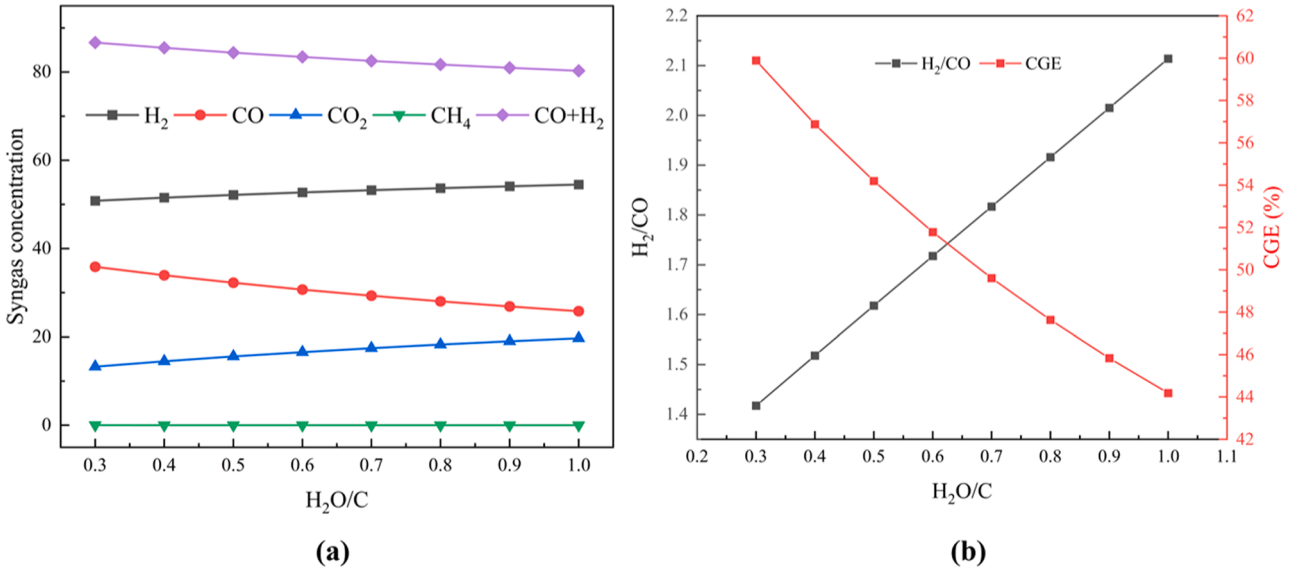

Fig. 4. Effect of H_2O/C on (a) Syngas Concentration, (b) H_2/CO, and CGE.

directly leads to a decrease in CGE. On the other hand, the H_2/CO significantly increases with rising H_2O/C. This change is explained by the intensified water-gas shift reaction at higher H_2O/C, which leads to a significant increase in H_2 generation and a reduction in CO production, thus greatly enhancing the H_2/CO. These findings suggest that altering the H_2O to carbon ratio can significantly affect the outcomes of the gasification process, leading to increased H_2 production and a more favorable syngas composition. However, it is crucial to maintain a proper balance between the increase in H_2 production and the decrease in CGE to enhance the overall efficiency of the gasification process. Consequently, a H_2O/C of 0.6 is considered optimal.

3.2.3. *Effect of O/C*

Fig. 5 displays the trends in the molar fractions of syngas components, CGE, Y, and net heat power during the FWCLG process as the O/C increases from 1.0 to 2.0. Fig. 5**(a)** shows the changes in the molar fractions of each syngas component as the O/C varies between 1.0 and 2.0. With a gradual increase in O/C, the molar fraction of CO continuously decreases due to the provision of more lattice oxygen in the reaction system, which facilitates further oxidation of CO to CO_2. Consequently, the molar fraction of CO_2 gradually increases. As the O/C rises, the molar fraction of H_2 also decreases because, in a high O/C environment, H_2 is more likely to be oxidized to H_2O. The molar fraction of CH_4 remains relatively stable across the range of O/C. As the O/C increases, the molar fractions of CO and H_2 decline, indicating that at high O/C conditions, more syngas is converted into non-combustible CO_2 and H_2O, leading to an overall reduction in the molar fractions of combustible gases.

Fig. 5**(b)** describes the trends in CGE, Y, and net heat power of the system as the O/C varies from 1.0 to 2.0. CGE gradually decreases with increasing O/C, a trend consistent with the changes in the molar fractions of syngas components. This indicates that higher O/C lead to more complete oxidation reactions, reducing the production of combustible gases and thus lowering CGE. Y also decreases with increasing O/C, as syngas primarily composed of CO and H_2 sees reduced molar fractions of both components at higher O/C. Conversely, the net heat power of the system gradually increases with higher O/C because more exothermic complete oxidation reactions (such as the oxidation of CO to CO_2 and H_2 to H_2O) occur under high O/C conditions, releasing more heat and thereby increasing the system's net heat power. Therefore, while higher O/C increase the system's net heat power, they also lead to decreases in CGE and Y. This underscores the need to balance these factors when optimizing system performance. Hence, an O/C of 1.5 is considered more suitable, at which the system achieves an H_2/CO of 1.718, a yield of 1.209 m^3/kg, and a CGE of 51.78 %.

3.2.4. *Hydrogen production rates in different regions*

The composition of FW from various locations may influence hydrogen production in the FWCLG process. This section explores the impact of differing FW compositions from various regions in China on hydrogen output. Table 2 presents the breakdown of FW composition from these regions, while Fig. 4 illustrates hydrogen production variations in the FWCLG process with different FW compositions. Despite these variations, Fig. 4 demonstrates that hydrogen concentration in the syngas produced by the FWCLG process shows minimal regional variation. This observed variance can be attributed to geographical factors, such as dietary habits, which influence the composition of food waste. However, within certain limits, these differences have a negligible impact on hydrogen production.

Data from Table 2 indicates that the hydrogen content in syngas largely depends on the hydrogen content in the FW. In Beijing, the hydrogen yield is slightly lower than in Qingdao, attributed to the higher carbon content in Beijing's FW. This higher carbon content leads to increased OC entering the reactor, where excess OC may consume additional hydrogen, reducing the hydrogen yield. As expected, regional differences in sulfur content in FW contribute to variations in hydrogen sulfide levels in the syngas. Nevertheless, the overall composition of FW remains fairly consistent across different regions, as starch is a common staple. Variations in FW composition is primarily influenced by local preferences for side dishes. For instance, Qingdao, a coastal city, has a preference for seafood, which significantly increases the sulfur content in the FW of the region.

4. Life cycle assessment

In the FWCLG process, several positive environmental impacts are generated. However, quantifying the environmental changes caused by FWCLG systems in different regions remains a significant challenge. Life Cycle Assessment (LCA) serves as a vital tool in this context, providing an objective depiction of the environmental impacts of FWCLG systems across various regions. The framework set by the International Organization for Standardization (ISO) categorizes environmental impacts into five key areas: global warming, acidification, eutrophication, photochemical ozone production, and particulate matter.

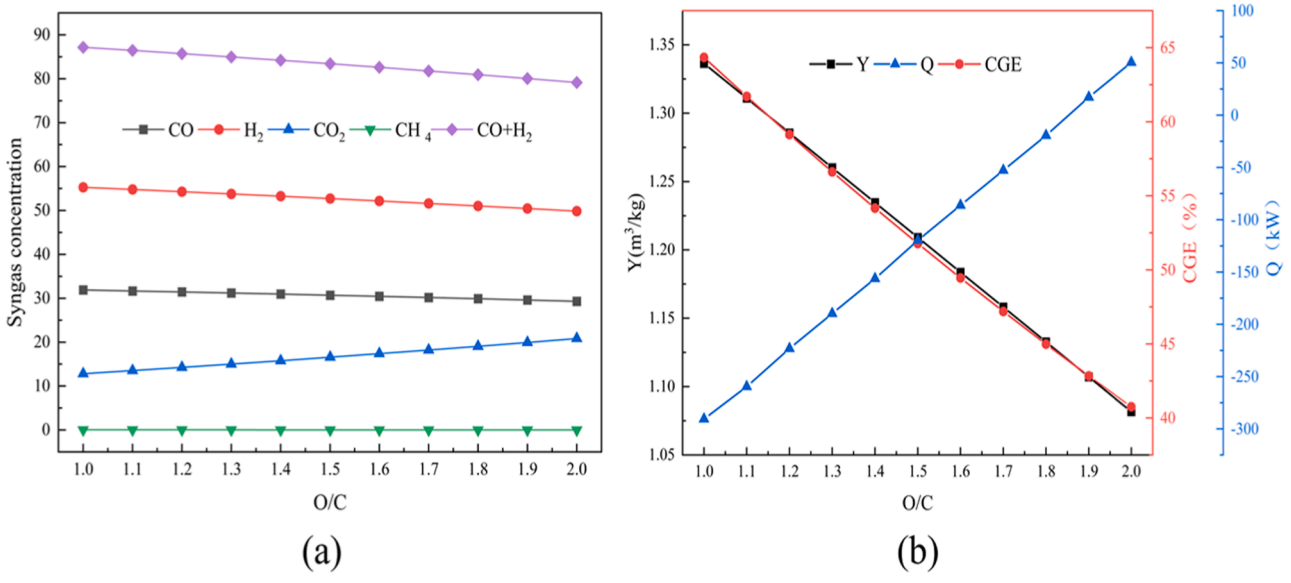

Fig. 5. Effect of O/C on (a) Syngas Concentration, (b) H_2/CO, CGE, and Net Heat Power.

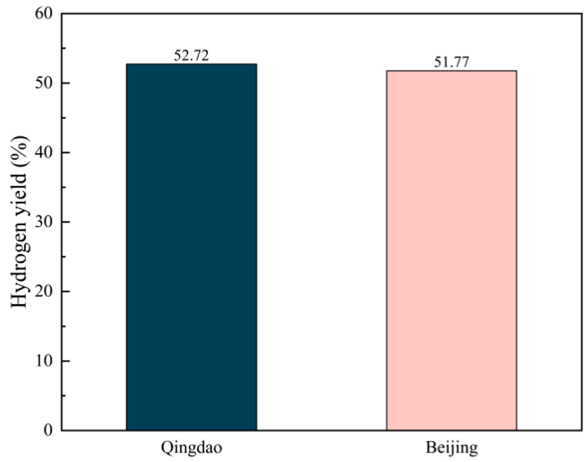

Fig. 6. Hydrogen Yield of FWCLG in Different Regions.

To quantify the environmental impacts from two different perspectives, researchers employed the Ecochain LCA software to analyze the environmental aspects of the process. Conducting an LCA requires adherence to a specific framework and sequence of activities. These are divided into four principal stages: defining the goals and scope, conducting an inventory analysis, performing an impact assessment, and interpreting the results (Rebitzer et al., 2004).

4.1. Definition of goal and scope

The CLG process for FW is a complex procedure involving multiple coupled chemical reactions. It encompasses various inputs of production materials and consumption of terminal energy and involves the formation of multiple intermediate products and the output of several products, thus creating a complex product symbiosis system. Therefore, defining the subject and determining the assessment scope of the LCA is not only the initial step in conducting LCA research but also lays the foundation for subsequent evaluations.

The primary goal of FWCLG is to facilitate the utilization of clean energy to replace fossil fuels. This includes a comprehensive analysis of the entire life cycle of the product, focusing on clean energy utilization, greenhouse gas emissions, and other environmental impact factors. The system follows a "cradle-to-gate" LCA approach. According to the ISO 14040 standard requirements (Klüppel, 2005), the analysis is conducted using Ecochain LCA software. The system boundary is established based on the European Union Product Environmental Footprint guidelines, which suggest excluding processes whose material, energy, and environmental significance do not exceed 3 %. The system boundary is illustrated in Fig. 7.

Assuming a 25 years operational lifespan for the system, the environmental impact of the initial construction and installation phases of the CLG plant is relatively limited and can be considered negligible when compared to the duration of the entire operational period. Consequently, when defining the system boundary for the LCA, phases such as plant construction, equipment manufacturing, and installation are excluded based on the cut-off criteria. Furthermore, greenhouse gas emissions and energy consumption during the production of construction materials and infrastructure development are also excluded from the environmental impact calculations.

The ash resulting from the FW is collected and transported to a landfill, while the airborne particles and smoke are categorized as fly ash and ashes. Once the system boundary is established, it becomes necessary to define the functional unit of the system to facilitate the subsequent life cycle inventory analysis. Inventory data are then adjusted according to the functional unit to determine the energy consumption and environmental emission intensity indicators for the entire process. The functional unit for the LCA of this system is defined as the treatment of 1 t of FW.

4.2. Life cycle inventory

Assuming a theoretical distance of 50 km between the waste treatment facility and the CLG plant, FW is transported to the CLG plant, while bottom ash and fly ash are disposed of in a landfill. In China, the average fuel consumption rate for road transportation is 0.067 L/(t/km). The LHV of diesel is 46.04 MJ/kg, with a density of 0.83 kg/L (Liang et al., 2011). Transporting FW in a 16 t truck results in gas emissions due to diesel fuel consumption. Table 4 outlines the energy consumption and gas emissions associated with the transportation of FW and ash, based on the aforementioned assumptions. Additionally, Table 5 details the LCA inventory for processing 1 t of FW, including

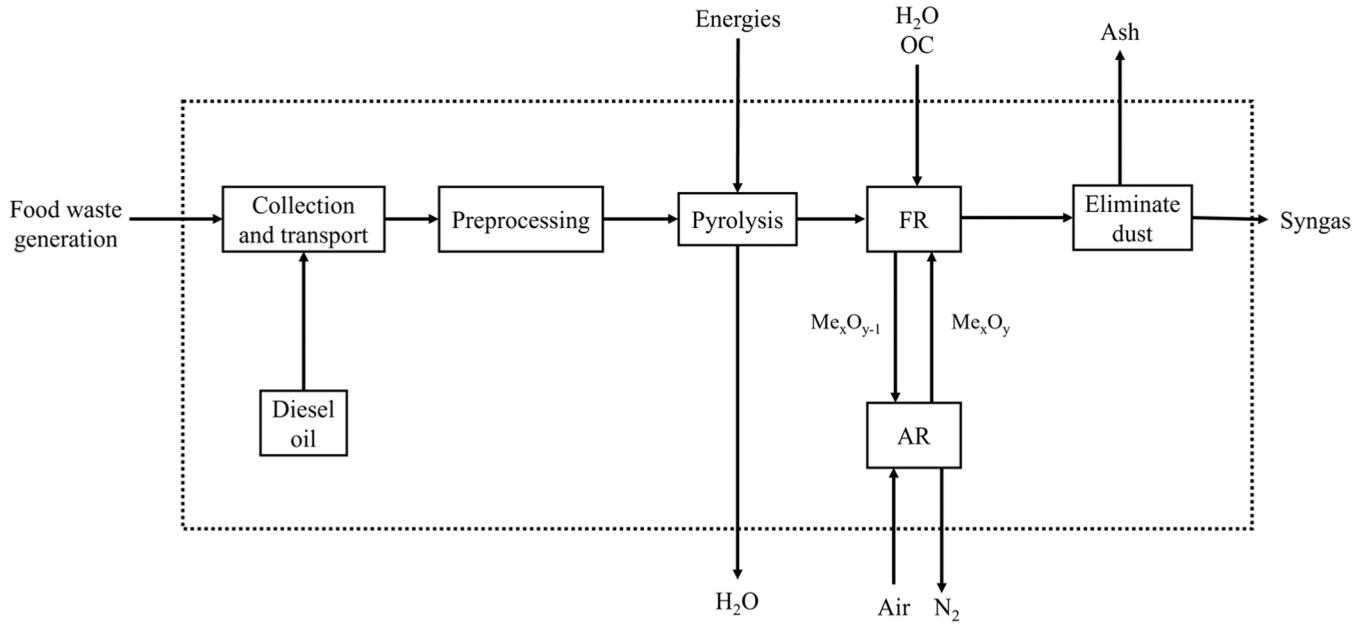

Fig. 7. System Boundary for the Life Cycle Assessment of the FWCLG System.

Table 4
Energy Consumption and Emissions During the Transportation of Municipal Solid Waste and Ash.

Energy Consumption	Exhaust emissions (g/t FW)							
Diesel oil	VOC	CO	NO_X	PM_{10}	SO_X	CH_4	N_2O	CO_2
2.7805	8.522	45.27	92.86	1.881	4.427	0.4427	0.5534	14035.06

Table 5
List of LCA per t of FW handled in different areas.

	Item	Unit	Qingdao	Beijing	Source
Importation	FW	Kg	1000	1000	Aspen
	OC	Kg	6412.66	6993.9	Aspen
	Water	Kg	368.82	381.07	Aspen
	Energy	KW	2095.04	1751.00	Aspen
	Diesel oil	Kg	2.78	2.78	Ecochain
	Electrical	kWh	20.04	17.80	Aspen
Exports	CO	Kg	556.05	607.77	Aspen
	CO_2	Kg	471.65	468.73	Aspen
	CH_4	Kg	0.15	0.64	Aspen
	NO_X	Kg	0.55	0.80	Aspen
	SO_2	Kg	4.43	6.40	Aspen
	HCL	Kg	-	-	-
	H_2S	Kg	6.36	3.93	Aspen
	HF	Kg	-	-	-
	COD	Kg	4.06	3.06	Ecochain
	VOC	Kg	12.32	3.56	Ecochain
	PM_{10}	Kg	11.23	44.88	Ecochain

data on energy consumption and emissions from transporting municipal solid waste and ash.

From Table 5, it is evident that when processing 1 t of FW, the FWCLG process in Qingdao yields relatively higher amounts of H_2S, COD, and VOC compared to the process in Beijing. As a coastal city, Qingdao's higher seafood consumption contributes to the generation of more organic compounds and pollutants during gasification. Conversely, the PM_{10} produced by the FWCLG process in Qingdao is lower than that in Beijing, which significantly mitigates smog conditions. This indirectly suggests that Beijing experiences more smog from waste incineration compared to Qingdao.

4.3. Life cycle characterization

The emissions detected during the inventory phase were categorized into five distinct environmental impact categories: global warming (GW), acidification (AC), nutrient enrichment (NE), photochemical ozone production (PO), and soot and ashes (SA). This classification follows the methodologies provided by the Research Center for Eco-Environmental Sciences, Chinese Academy of Sciences (Tang et al., 2013). During the characterization phase, the quantified effect of each emission on different environmental categories is assessed. Characterization is determined by the properties of the released compounds, and the characterization variables found in existing literature are applicable worldwide (Liang et al., 2011). The comprehensive characterization data are provided in Table 6.

Chemicals such as CO_2, CH_4, NO_x, and CO all have the potential to trigger global warming, measured in kilograms of carbon dioxide equivalent ($kgCO_{2\text{-eq}}$). The GWP values of FWCLG in Qingdao and Beijing reach 1763.5 and 1956.27 $kgCO_{2\text{-eq}}$, respectively. Among the global warming effects, CO emissions produce the most significant impacts, followed closely by CO_2. Compared to CO and CO_2, the overall impact of CH_4 and NO_x on global warming is more limited, mainly because this model treats a functional unit of 1 t of FW instead of syngas.

Regarding environmental acidification, chemicals such as SO_2, NO_x, H_2S, HCl, and HF have the potential to cause this phenomenon. Acidification values are described in terms of kilograms of sulfur dioxide equivalent ($kgSO_{2\text{-eq}}$). During acidification, H_2S has the most significant effect, followed by SO_2, while NO_x has a relatively mild effect. Nutrient enrichment and photochemical ozone production are described by kg-equivalents of PO_4 and C_2H_4, respectively. In this study, the role of CH4 in photochemical ozone production can be ignored.

4.4. Normalization and weighting

During the normalization process, the environmental impact of each factor is divided by the estimated lifespan of the product and the average annual contribution of each impact per individual. In the weighting stage, researchers assign weights to the data obtained from the normalization step, considering the varying significance of different environmental influences and their specific emphasis on the studied impacts. Weighting variables are used to accurately represent the relative significance of different environmental consequences. Despite extensive data collection efforts nationwide, gaps remain in domestic

Table 6
Values of Different Environmental Impact Categories for Processing 1 t of FW in Different Regions.

Environmental impacts	Name of substance	Total emissions (kg)		Equivalent factor	Equivalent mass	
		Qingdao	Beijing		Qingdao	Beijing
GW	CO_2	471.65	468.73	1	471.65	468.73
	CO	556.05	607.77	2	1112.1	1215.54
	CH_4	0.15	0.64	25	3.75	16
	NO_X	0.55	0.8	320	176	256
	Total ($kgCO_{2\text{-eq}}$)				1763.5	1956.27
AC	SO_2	4.43	6.4	1	4.43	6.4
	NO_X	0.55	0.8	0.7	0.385	0.56
	HCI	0	0	0.88	0	0
	H_2S	6.36	3.93	1.88	11.9568	7.3884
	HF	0	0	1.6	0	0
	Total ($kgSO_{2\text{-eq}}$)				16.7718	14.3484
NE	NO_X	0.55	0.8	1.35	0.7425	0.7425
	COD	4.06	3.06	0.23	0.9338	0.7038
	Total ($kgPO_{4\text{-eq}}$)				1.6763	1.4463
PO	VOC	12.32	3.56	0.6	7.392	2.136
	CO	556.05	607.77	0.03	16.6815	18.2331
	CH_4	0.15	0.64	0.007	0.00105	0.00448
	Total ($kgC_2H_{4\text{-eq}}$)				24.07455	20.37358
SA	PM_{10}	11.23	44.88	1	11.23	44.88

inventory data. For climate change and ozone depletion contexts, the latest emission data for HFCs and CFCs are taken from the literature (Tang et al., 2013).

However, for inventory data related to ionizing radiation and toxic chemicals, emission data are currently unavailable from existing literature or databases. Weighted environmental impact potential values are obtained through weighting, with units in person-equivalents (target year), denoted as PET. The normalization references and weighting factors (WF(j)) differ across nations. This research utilizes the data documented by Chen and Huang (Yang and Nielsen, 2001).

The formula used to compute the weighted environmental potential (WP(j)) for China is as follows:

$$WP(j) = \frac{EP(j)}{TgER(j)} gWF(j)\# \tag{15}$$

The equation represents the relationship between the environmental effect potential (EP(j)) of a certain impact category (j), the life expectancy of the product (T) in years, and the normalized reference value of emissions (ER(j)) for that impact category.

Table 7 presents a summary of the findings on the weighted environmental potential (WP) for several areas of environmental impact. The WP(j) values for FWCLG in Qingdao and Beijing are 15.67 PET and 22.13 PET, respectively. From an environmental impact perspective, FWCLG in Beijing performs better than in Qingdao. This is primarily due to the higher proportion of organic matter in Qingdao FW, including vegetable, seafood, and fruit residues. These organic materials may produce more pollutants, such as VOCs, CO, and other harmful gases during the gasification process. Additionally, as a coastal city, Qingdao food waste tends to have higher moisture content, which can reduce the efficiency of the gasification process, increase energy consumption, and result in more pollutant generation.

There are significant differences in the WP(j) values for their impact on GW. As shown in Fig. 8, for FWCLG plants in both cities, PO and SA have the greatest impact over their life cycles. For PO, this is mainly due to the selected functional unit of processing 1 t of municipal waste; if the functional unit were changed to producing 1 t of syngas, the impact would be greatly reduced.

Although some pollutants produced during the gasification of food waste in Qingdao are relatively high, the overall environmental impact is smaller. CLG technology offers an effective and environmentally friendly waste treatment solution for Qingdao by efficiently recovering energy, reducing pollutant emissions, lowering greenhouse gas emissions, handling diverse types of waste, and providing good economic benefits.

5. Economic analysis

The techno-economic model of the FWCLG system is solved by calculating the Total Capital Investment (TCI) and the Total Production Cost (TPC). The economic benefits of the FWCLG process are evaluated using techno-economic indicators, such as Return on Investment (ROI), Payback Period (PBP), and Net Present Value (NPV). The assumptions listed in Table 8 are utilized to compute the economic efficacy of the system implemented in this study.

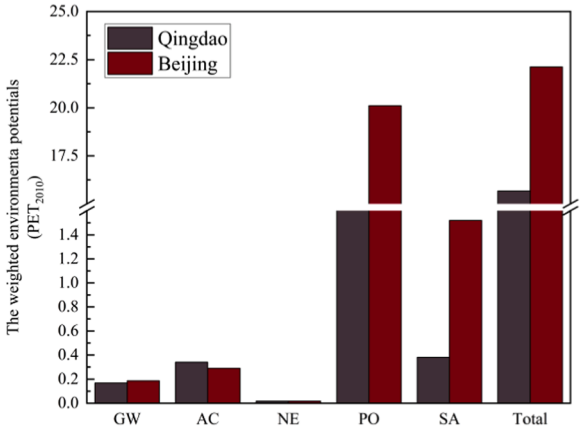

Fig. 8. Weighted environmental potential of 1 t FWCLG for different cities.

Table 8
Economic Analysis Assumptions.

Item	Numerical value
Base year	2020
Total hours of operation per year, h	7200
Planned year of operation	25
Duty rate	25 %
Cross-subsidies	10 %
H_2 price, $/kg	5

5.1. Total capital investment

The TCI for an industrial plant consists of two main parts: the Fixed Capital Investment (FCI) and the Working Capital (WC) (Orhan et al., 2008). FCI refers to the investment required for providing plant facilities and necessary manufacturing, including both direct and indirect investments. WC, on the other hand, represents the investment needed to commence plant operations, encompassing components such as finished products, taxes, and other expenses (Liu et al., 2017). Various methods are available to calculate TCI depending on the level of detail and accuracy required (Cabello et al., 2019). In this study, the percentage delivered-equipment method is used to calculate the TCI. By considering the ratio of the cost of the purchased equipment, it is possible to determine the other investments that comprise the TCI. Table 9 displays the constituents of TCI and their corresponding ratios.

The cost of purchased equipment can be estimated using Eq. (16) (Zhang, 2009).

$$I_{2020} = I_{ref} \times \left(\frac{Q}{Q_{ref}}\right)^n \times \frac{CEPCI_{2020}}{CEPCI_{ref}}\# \tag{16}$$

The variable i represents the monetary value allocated for the purchase of equipment in the reference scenario. I_{2020} represents the monetary obligation undertaken for the acquisition of equipment in the year 2020. The term scaling exponent denotes a mathematical exponent. Q represents the research project capability, while also symbolizing the

Table 7
Weighted Environmental Potential for Different Environmental Impact Categories.

Impact category	Equivalent mass		Normalization reference	Weighting factor	Weighted environment potential (PET)	
	Qingdao	Beijing			Qingdao	Beijing
GW	1763.5	1956.27	8700 $kgCO_{2\text{-eq}}$/(person·a)	0.83	0.1682	0.1866
AC	16.77	14.35	36 $kgSO_{2\text{-eq}}$/(person·a)	0.73	0.34	0.291
NE	1.446	1.446	61 $kgPO_{4\text{-eq}}$/(person·a)	0.73	0.01731	0.01731
PO	18.82	25.63	0.65 $kgC_2H_{4\text{-eq}}$/(person·a)	0.51	18.89	15.99
SA	11.23	44.88	18 kg/(person·a)	0.61	0.3806	1.521
Total					19.8	18.00

Table 9
Components of TCI and Their Respective Proportions (Yang et al., 2016; Zhou et al., 2016).

Component	Range (%)	Assumption (%)
(A) Direct investment		
Purchased equipment	16–40	30
Piping	3–9	5
Purchased equipment installation	7–14	8
Buildings	5–16	12
Electrical systems	2–10	6
Land	1–2	1
Instrumentation and controls	2–7	5
(B) Indirect investment		
Project contractual costs	2–7	5
Plant construction costs	4–18	10
Construction Engineering Supervision	4–19	11
Project contingency	5–17	7
(C) Fixed capital investment	(A)+ (B)	100
(D) Working capital	10–20	15
(E) Total capital investment	(C)+ (D)	115

reference project capability. The term $CEPCI_{ref}$ represents the Chemical Engineering Plant Cost Index in the reference instance, while $CEPCI_{2020}$ specifically refers to the CEPCI value for the year 2020.

Specifically, the CEPCI adjusts past equipment investments to the present by accounting for monetary data changes due to inflation and deflation. The values for n, I_{ref}, $CEPCI_{ref}$ and Q_{ref} are provided in Table 10, with the value of $CEPCI_{2020}$ being 596.2.

5.2. Total production costs

The TPC encompasses expenditures related to administration, utilities, maintenance and operation, depreciation, raw materials, sales and distribution, and plant management expenses. Table 11 displays the fundamental assumptions used in the computation of TPC. The system was assessed using the projected data of the FWCLG system. Additionally, given a residual value of 4 % and a lifetime of 25 years, the straight-line method was suggested for calculating the depreciation value (Okoli and Adams, 2014). The values of the remaining parameters in TPC were calculated based on their respective proportions in the TPC (Qian et al., 2014).

5.3. Profitability analysis

The profitability of the FWCLG process is reflected by ROI, PBP, and NPV. According to Eq. (17) (Qian et al., 2014), ROI is defined as the ratio of Profit After Tax (PAT) to TCI. PBP is represented by FCI, PAT, and Depreciation (D), as shown in Eq. (18) (Cho et al., 2013). NPV is calculated using the After-Tax Cash Flow (ATCF), discount rate (a), plant lifetime (b), and TCI, according to Eq. (19) (Yao et al., 2017).

Table 10
Reference Case for Purchased Equipment Investment (Campanari et al., 2014; Khan and Shamim, 2016)。.

Equipment	Benchmark	$CEPCI_{ref}$	Q_{ref}	I_{ref} ($\times 10^6$ $)	n
FR	Moderator	541.7/2016	40 kg/s	1.23/2016	0.67
AR	Atmosphere	541.7/2016	59.4 kg/s	0.629/2016	0.67
Cyclone	OC mass flow rate	541.7/2016	280.5 kg/s	0.0693/2016	0.67
Clean up	Detergent flow rate	468.2/2005	0.29 kmol/s	7.1/2005	0.74
Heat exchangers	Heat exchange	576.1/2014	57.20 MW	1.639/2014	0.9

Table 11
TPC Assumptions for Economic Analysis of the FWCLG System.

Parameter	Assumption
(A) Cost of raw materials	OC: 320 $/t (data sourced from manufacturer), Water: 0.7608 $/t
(B) Utility costs	Water: 0.7608 $/t, Electricity: 0.0075 $/kWh (Xiang et al., 2014)
(C) Operation and Maintenance Costs	
(a) Operational labor costs	20 labors (1.04×10^5 $/labor/year)(Zhou et al., 2022)
(b) Direct supervision and paperwork costs	20 % of operating labor costs
(c) Maintenance and repair costs	2 % of FCI
(d) Cost of operating supplies	0.7 % of FCI
(e) Cost of laboratory fees	15 % of operating labor costs
(D) Depreciation cost	Lifetime 25 years; salvage value 4 %
(E) Plant construction costs Investment costs	60 % of (a)+ (b)+ (c)
(F) Distribution and cost of sales	2 % of (H)
(G) Administrative input costs	2 % of (H)
(H) Total production cost	(A)+ (B)+ (C)+ (D)+ (E)+ (F)+ (G)

$$ROI = \frac{PAT}{TCI}\# \tag{17}$$

$$PBP = \frac{FCI}{PAT + D}\# \tag{18}$$

$$NPV = ATCF \times \left[\frac{(1+\alpha)^{\beta} - 1}{\alpha \times (1+\alpha)^{\beta}}\right] - TCl\# \tag{19}$$

5.4. Economic indicator

The FCI, WC, and TCI are assessed using the percentages shown in Table 12, which are derived from the equipment investment. The FCI value is 3.25×10^6 $, the WC value is 1.069×10^6 $, and the TCI value is 0.1545×10^6 $. Based on the assumptions provided in Table 8, we have calculated the TPC and the production cost of H_2. The results of these calculations are shown in Table 12. The TPC of H_2 is 1.118×10^6 per year, whereas the cost of producing one kilogram of H_2 is $2.104. The ROI, PBP, and NPV are computed using Eqs. (4) and (6). The ROI is 11.23 %, the PBP is 6.283 years, and the NPV is 1.201×10^6 $.

Additionally, the distribution of hydrogen production costs is illustrated in Fig. 9. Maintenance and operation costs account for the largest proportion of these costs, at 38.3 %. Therefore, it is essential to formulate and implement a preventive maintenance plan, which includes regular inspections and upkeep of equipment. This approach helps detect and address potential issues promptly, thereby avoiding high repair costs due to equipment failures. Using high-quality materials and components can extend the lifespan of equipment and reduce

Table 12
TCI, TPC, ROI, PBP, and NPV Values for the FWCLG Process in 2020.

Items	Value
FCI($\times 10^6$ $)	3.25
WC($\times 10^6$ $)	1.069
TCI($\times 10^6$ $)	0.1545
Depreciation($\times 10^6$ $/year)	0.1247
TPC($\times 10^6$ $/year)	1.118
H_2 production cost ($/kg)	2.104
Revenue($\times 10^6$ $/year)	2.686
Profit before tax($\times 10^6$ $/year)	1.569
Tax rate	25 %
PAT($\times 10^6$ $/year)	0.3922
ATCF($\times 10^6$ $/year)	0.5171
ROI	11.23 %
PBP (years)	6.283
NPV($\times 10^6$ $)	1.201

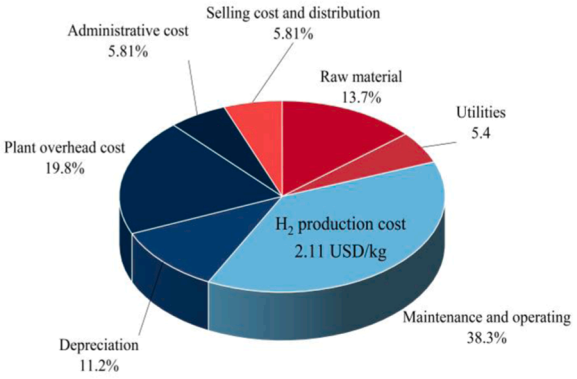

Fig. 9. Breakdown of Hydrogen Production Costs for FWCLG.

maintenance frequency, making it an effective strategy for maintaining stable hydrogen production costs.

5.5. Sensitivity studies

Fig. 10 presents a sensitivity analysis identifying key cost drivers for hydrogen production. The selected parameters are OC price, OC makeup ratio, water price, equipment lifespan, and operating labor. Based on assumed parameters reported in the literature, each parameter is varied by ± 20 % from the baseline (Li et al., 2020). OC price, OC makeup ratio, water price, and operating labor show a positive correlation with hydrogen production costs, while equipment lifespan shows a negative correlation. Operating labor has the most significant impact. When labor costs vary within ± 20 % (from 9320 $/labor/year to 12480 $/labor/-year), hydrogen production costs range from 1.91 $/kg to 2.30 $/kg. The impacts of OC price and OC makeup ratio are almost identical. A decrease in OC price (from 320 $/t to 256 $/t) lowers hydrogen production costs (from 2.104 $/kg to 2.05 $/kg). Additionally, water price has the least impact. A reduction in water price (from 0.7714 $/t to 0.6171 $/t) results in a decrease in hydrogen production costs (from 2.104 $/kg to 2.09 $/kg).

5.6. Comparative analysis with other processes

Fig. 11 compares the production cost of hydrogen with that of other industrial processes. According to Li et al.(Li et al., 2020), in the year

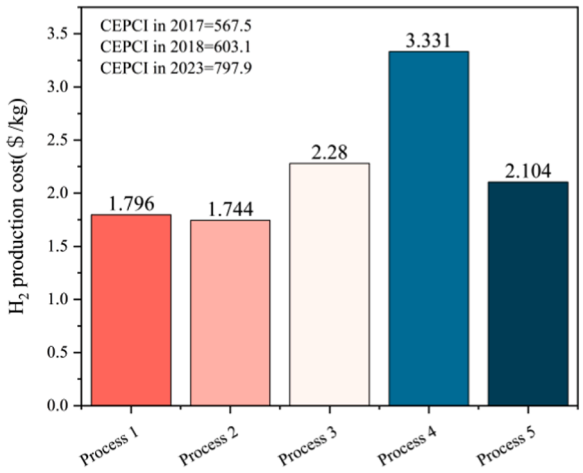

Fig. 11. Comparison of Hydrogen Production Costs for Different Processes.

2020, the cost of producing hydrogen utilizing iron-based oxygen carriers in coal CLG was 1.71 $/kg (Process 1). In 2018, Khan et al. (Khan and Shamim, 2019) found that the cost of producing hydrogen using natural gas chemical looping reforming employing iron-based oxygen carriers was 1.66 $/kg (Process 2). Wu et al. (Wu et al., 2024) reported that the cost of producing hydrogen from biomass CLG in 2023 (the reference year) was 3.05 $/kg (Process 3). In 2018, Liu et al. (Liu et al., 2020) conducted a study on the cost of producing hydrogen from renewable energy sources. They determined that the cost was 3.37 $/kg, specifically referring to Process 4. The hydrogen production cost for Process 5 in 2020 was $2.104 per kilogram. The hydrogen production costs were computed in several reference years and then adjusted for inflation to 2020 using the Hydrogen Production Cost Index (HPC) (Li et al., 2020)。

$$HPC_{2020} = HPC_{ref} \times \frac{CEPCI_{2020}}{CEPCI_{ref}} \# \tag{20}$$

Fig. 11 illustrates a comparison of the expenses associated with hydrogen production using various techniques. The comparison reveals that the hydrogen production cost for Process 1 is 1.796 $/kg, which is relatively low due to the inexpensive cost of coal and the advanced state of the technology. Process 2 has the most economical hydrogen generation cost, amounting to 1.744 $/kg, primarily due to the consistent and

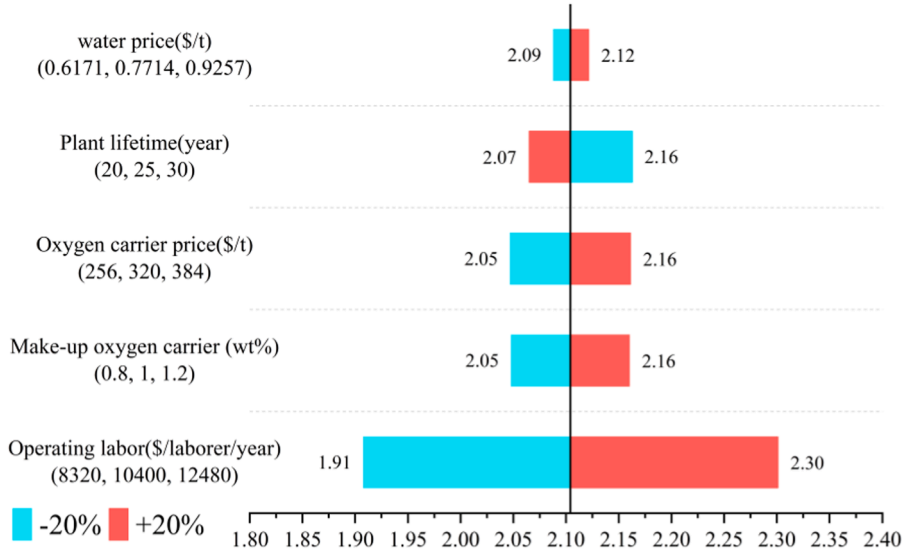

Fig. 10. Sensitivity study of the effect of variables on the cost of hydrogen production.

affordable price of natural gas. The cost of producing hydrogen for Process 3 is 2.28 $/kg, driven by the complexity of its collection and treatment process, although it offers environmental benefits. Process 4 has the highest hydrogen production cost, at 3.331 $/kg, mainly due to the significant expenses associated with initial investment and infrastructure construction.

The current FWCLG process has a hydrogen production cost of 2.104 $/kg, which is notably lower than the cost of hydrogen production from renewable energy sources. Utilizing FW as a raw material not only reduces the burden of waste disposal but also optimizes the utilization of waste resources. The low acquisition cost and intricate treatment process of this method yield substantial environmental and social advantages. Thus, FWCLG hydrogen generation has a comprehensive advantage in terms of both cost and environmental impact, making it highly attractive for future applications.

6. Conclusion

The study utilized Aspen Plus process simulation software to model a 10 MW_{th} FWCLG hydrogen production system. A sensitivity analysis was performed to determine the most favorable settings for the system. Additionally, a comprehensive examination of the technology lifetime and economic analysis was conducted to systematically evaluate its viability and benefits in real-world applications. The primary findings can be summarized as follows:

(1) The gasification process was elucidated by analyzing the impact of various operating factors using Aspen Plus software simulation. According to the study, when the temperature of the FR is 850°C, the H_2O/C is 0.6, and the O/C is 0.45, the system achieves an H_2/CO of 1.718, a Y of 1.209 m^3/kg, and a CGE of 51.78 %.
(2) The LCA determined that the system in Qingdao had a GWP of 1763.5 $kgCO_{2\text{-eq}}$ and 16.77 $kgSO_{2\text{-eq}}$. Although the gasification of FW in Qingdao results in increased generation of certain pollutants, the overall environmental impact is minimal. CLG technology is deemed more appropriate for waste treatment in Qingdao, facilitating efficient resource utilization and environmental protection objectives.
(3) A comprehensive economic review was performed to analyze the economic aspects of the 10 MW_{th} FWCLG hydrogen generation system. The findings demonstrate that the system yields favorable economic advantages, with a ROI of 11.23 %, a PBP of 6.283 years, and a NPV of 1.201×10^6 $. Hydrogen production using FWCLG is more cost-effective compared to renewable energy-based methods. Additionally, it provides significant environmental benefits by efficiently utilizing waste resources and reducing waste disposal pressure. The FWCLG hydrogen production technique holds significant potential for widespread implementation due to its favorable economic and environmental advantages.

CRediT authorship contribution statement

Tuo Guo: Writing – review & editing, Visualization, Validation, Formal analysis. **Qiuyan Xue:** Visualization, Data curation. **Mingyang Dai:** Writing – review & editing, Writing – original draft, Visualization, Validation, Software, Methodology, Investigation, Formal analysis, Data curation, Conceptualization. **Qingjie Guo:** Writing – review & editing, Supervision, Project administration, Funding acquisition.

Declaration of Competing Interest

The authors declare that they have no known competing financial interests or personal relationships that could have appeared to influence the work reported in this paper.

Acknowledgments

The authors are very grateful to the Natural Science Foundation Project of Ningxia (2022AAC01001) and National Natural Science Foundation of China (U20A20124 and 22379079).

Appendix A. Supporting information

Supplementary data associated with this article can be found in the online version at doi:10.1016/j.psep.2024.12.103.

References

Ahmed, I., Gupta, A., 2010. Pyrolysis and gasification of food waste: Syngas characteristics and char gasification kinetics. Appl. Energ. 87, 101–108.
Al-Malah, K.I., 2022. Aspen plus: chemical engineering applications. John Wiley & Sons.
Cabello, A., Hughes, R.W., Symonds, R.T., Champagne, S., Lu, D.Y., Mostafavi, E., Mahinpey, N., 2019. Economic analysis of pressurized chemical looping combustion for steam assisted gravity drainage applications. Int J. Greenh. Gas. Con 90, 102786.
Campanari, S., Chiesa, P., Manzolini, G., Bedogni, S., 2014. Economic analysis of CO_2 capture from natural gas combined cycles using Molten Carbonate Fuel Cells. Appl. Energ. 130, 562–573.
Caton, P., Carr, M., Kim, S., Beautyman, M., 2010. Energy recovery from waste food by combustion or gasification with the potential for regenerative dehydration: A case study. Energ. Convers. Manag. 51, 1157–1169.
Chen, P., Sun, X., Gao, M., Ma, J., Guo, Q., 2019. Transformation and migration of cadmium during chemical-looping combustion/gasification of municipal solid waste. Chem. Eng. J. 365, 389–399.
Cho, H.J., Kim, J.-K., Cho, H.-J., Yeo, Y.-K., 2013. Techno-economic study of a biodiesel production from palm fatty acid distillate. Ind. Eng. Chem. Res. 52, 462–468.
Desgagnés, A., Iliuta, I., Iliuta, M.C., 2024. Sorption-enhanced intensified CO_2 hydrogenation via reverse water–gas shift reaction: Kinetics and modelling. Chem. Eng. J., 152052
Dhiman, S., Mukherjee, G., 2021. Present scenario and future scope of food waste to biofuel production. J. Food Process Eng. 44, e13594.
Dieringer, P., Marx, F., Alobaid, F., Ströhle, J., Epple, B., 2020. Process control strategies in chemical looping gasification—a novel process for the production of biofuels allowing for net negative CO_2 emissions. Appl. Sci. 10, 4271.
Havukainen, J., Zhan, M., Dong, J., Liikanen, M., Deviatkin, I., Li, X., Horttanainen, M., 2017. Environmental impact assessment of municipal solid waste management incorporating mechanical treatment of waste and incineration in Hangzhou, China. J. Clean. Prod. 141, 453–461.
Jiang, Q., Li, T., He, Y., Wu, Y., Zhang, J., Jiang, M., 2022. Simultaneous removal of hydrogen sulfide and ammonia in the gas phase: a review. Environ. Chem. Lett. 1–17.
Jin, C., Sun, S., Yang, D., Sheng, W., Ma, Y., He, W., Li, G., 2021. Anaerobic digestion: An alternative resource treatment option for food waste in China. Sci. Total Environ. 779, 146397.
Khan, M.N., Shamim, T., 2016. Techno-economic assessment of a plant based on a three reactor chemical looping reforming system. Int J. Hydrog. Energ. 41, 22677–22688.
Khan, M.N., Shamim, T., 2019. Techno-economic assessment of a chemical looping reforming combined cycle plant with iron and tungsten based oxygen carriers. Int J. Hydrog. Energ. 44, 11525–11534.
Klüppel, H.-J., 2005. The Revision of ISO Standards 14040-3-ISO 14040: Environmental management–Life cycle assessment–Principles and framework-ISO 14044: Environmental management–Life cycle assessment–Requirements and guidelines. Int. J. Life Cycle Assess. 10, 165, 165.
Li, G., Chang, Y., Liu, T., Yu, Z., Liu, Z., Liu, F., Ma, S., Weng, Y., Zhang, Y., 2020. Hydrogen element flow and economic analyses of a coal direct chemical looping hydrogen generation process. Energy 206, 118243.
Li, Z., Xu, H., Yang, W., Zhou, A., Xu, M., 2019. CFD simulation of a fluidized bed reactor for biomass chemical looping gasification with continuous feedstock. Energ. Convers. Manag. 201, 112143.
Liang, Z., Ma, X., Lin, H., Tang, Y., 2011. The energy consumption and environmental impacts of SCR technology in China. Appl. Energ. 88, 1120–1129.
Liu, B., Liu, S., Guo, S., Zhang, S., 2020. Economic study of a large-scale renewable hydrogen application utilizing surplus renewable energy and natural gas pipeline transportation in China. Int J. Hydrog. Energ. 45, 1385–1398.
Liu, Y., Qian, Y., Zhou, H., Xiao, H., Yang, S., 2017. Conceptual design of the coal to synthetic natural gas (SNG) process based on BGL gasifier: modeling and techno-economic analysis. Energy Fuels 31, 1023–1034.
Matsakas, L., Gao, Q., Jansson, S., Rova, U., Christakopoulos, P., 2017. Green conversion of municipal solid wastes into fuels and chemicals. Electron J. Biotechn 26, 69–83.
Menacho, W.A., Mazid, A.M., Das, N., 2022. Modelling and analysis for biogas production process simulation of food waste using Aspen Plus. Fuel 309, 122058.
Molino, A., Chianese, S., Musmarra, D., 2016. Biomass gasification technology: The state of the art overview. J. Energy Chem. 25, 10–25.
Okoli, C., Adams, T.A., 2014. Design and economic analysis of a thermochemical lignocellulosic biomass-to-butanol process. Ind. Eng. Chem. Res. 53, 11427–11441.
Orhan, M., Dincer, I., Naterer, G., 2008. Cost analysis of a thermochemical Cu–Cl pilot plant for nuclear-based hydrogen production. Int J. Hydrog. Energ. 33, 6006–6020.

Qian, Y., Yang, Q., Zhang, J., Zhou, H., Yang, S., 2014. Development of an integrated oil shale refinery process with coal gasification for hydrogen production. Ind. Eng. Chem. Res. 53, 19970–19978.
Ramzan, N., Ashraf, A., Naveed, S., Malik, A., 2011. Simulation of hybrid biomass gasification using Aspen plus: A comparative performance analysis for food, municipal solid and poultry waste. Biomass-.-. Bioenerg. 35, 3962–3969.
Rebitzer, G., Ekvall, T., Frischknecht, R., Hunkeler, D., Norris, G., Rydberg, T., Schmidt, W.-P., Suh, S., Weidema, B.P., Pennington, D.W., 2004. Life cycle assessment: Part 1: Framework, goal and scope definition, inventory analysis, and applications. Environ. Int 30, 701–720.
Saqib, N.U., Sharma, H.B., Baroutian, S., Dubey, B., Sarmah, A.K., 2019. Valorisation of food waste via hydrothermal carbonisation and techno-economic feasibility assessment. Sci. Total Environ. 690, 261–276.
Shahabuddin, M., Alam, M.T., Krishna, B.B., Bhaskar, T., Perkins, G., 2020. A review on the production of renewable aviation fuels from the gasification of biomass and residual wastes. Bioresour. Technol. 312, 123596.
Sun, Z., Chen, X., Kuo, P.-C., Ding, L., Aziz, M., 2024. Co-feeding biomass and municipal solid waste for enhanced hydrogen and synthetic natural gas yields employing chemical looping process. Chem. Eng. J., 152487
Tahir, F., Saeed, M.A., Ali, U., 2023. Biomass energy perspective in Pakistan based on chemical looping gasification for hydrogen production and power generation. Int J. Hydrog. Energ.
Tanaka, M., Ozaki, H., Ando, A., Kambara, S., Moritomi, H., 2008. Basic characteristics of food waste and food ash on steam gasification. Ind. Eng. Chem. Res. 47, 2414–2419.
Tang, Y., Ma, X., Lai, Z., Zhou, D., Lin, H., Chen, Y., 2012. NO_x and SO_2 emissions from municipal solid waste (MSW) combustion in CO_2/O_2 atmosphere. Energy 40, 300–306.
Tang, Y., Ma, X., Lai, Z., Chen, Y., 2013. Energy analysis and environmental impacts of a MSW oxy-fuel incineration power plant in China. Energy Policy 60, 132–141.
Wang, D., Liu, Y., Wang, B., Guo, Q., 2018. Chemical looping gasification of kitchen waste for syngas production. J. Chem. Eng. Chin. Univ. 32, 229–236.
Wu, D., Gao, Z., Wu, S., Xiao, R., 2024. Negative net global warming potential hydrogen production through biomass gasification combined with chemical looping: Environmental and economic assessments. Int J. Hydrog. Energ. 66, 24–32.
Xiang, D., Yang, S., Liu, X., Mai, Z., Qian, Y., 2014. Techno-economic performance of the coal-to-olefins process with CCS. Chem. Eng. J. 240, 45–54.
Xu, Z., Qi, H., Yao, D., Zhang, J., Zhu, Z., Wang, Y., Cui, P., 2022. Modeling and comprehensive analysis of food waste gasification process for hydrogen production. Energ. Convers. Manag. 258, 115509.
Xu, Z., Zhou, Y., Yin, K., Zhang, J., Zhu, Z., Wang, Y., Cui, P., 2023. Exergy, techno-economic and environment analysis of food waste plasma gasification and syngas chemical looping processes. J. Clean. Prod. 386, 135835.
Yang, J.-x, Nielsen, P.H., 2001. Chinese life cycle impact assessment factors. J. Environ. Sci. 13, 205–209.
Yang, S., Liang, J., Yang, S., Qian, Y., 2016. A novel cascade refrigeration process using waste heat and its application to coal-to-SNG. Energy 115, 486–497.
Yao, J., Kraussler, M., Benedikt, F., Hofbauer, H., 2017. Techno-economic assessment of hydrogen production based on dual fluidized bed biomass steam gasification, biogas steam reforming, and alkaline water electrolysis processes. Energ. Convers. Manag. 145, 278–292.
Yu, Z., Yang, Y., Yang, S., Zhang, Q., Zhao, J., Fang, Y., Hao, X., Guan, G., 2019. Iron-based oxygen carriers in chemical looping conversions: A review. Carbon Resour. Convers. 2, 23–34.
Yuan, P., Guo, T., Pan, X., Hu, X., Ma, J., Xu, D., Zhou, Z., Guo, Q., Guo, X., 2023. Process optimization and thermodynamic analysis of autothermal coal chemical looping gasification industrial demonstration system. Fuel 334, 126667.
Zhang, J., 2009. Technical and economic assessment for IGCC with CCS. Tsinghua University, Beijing.
Zhang, Y., Zhou, A., Li, Z., Zhang, H., Xiong, Y., Xiao, R., Hu, Z., Wang, X., 2024. Numerical simulation analysis of biomass gasification and rich-H_2 production process in a downdraft gasifier. J. Energy Inst. 114, 101596.
Zhou, H., Meng, A., Long, Y., Li, Q., Zhang, Y., 2014. An overview of characteristics of municipal solid waste fuel in China: physical, chemical composition and heating value. Renew. Sust. Energ. Rev. 36, 107–122.
Zhou, H., Yang, S., Xiao, H., Yang, Q., Qian, Y., Gao, L., 2016. Modeling and techno-economic analysis of shale-to-liquid and coal-to-liquid fuels processes. Energy 109, 201–210.
Zhou, X., Li, G., Liu, F., Li, N., 2022. Production of ethanol from corn straw based on chemical looping gasification: Economic analysis. Bioresour. Technol. 360, 127568.